

Geophysical Research Letters

RESEARCH LETTER

10.1029/2021GL093875

Key Points:

- North American barometric-pumping efficiency potential increases with latitude until around 50°N and then decreases
- For similar latitudes, locations on the Pacific coast generally have lower potentials than on the Atlantic coast in North America
- Barometric-pumping efficiency potential becomes less variable further from the North American coastline

Supporting Information:

Supporting Information may be found in the online version of this article.

Correspondence to:

S. T. Avendaño,
savendano@lanl.gov

Citation:

Avendaño, S. T., Harp, D. R., Kurwadkar, S., Ortiz, J. P., & Stauffer, P. H. (2021). Continental-scale geographic trends in barometric-pumping efficiency potential: A North American case study. *Geophysical Research Letters*, 48, e2021GL093875. <https://doi.org/10.1029/2021GL093875>

Received 14 APR 2021

Accepted 1 JUL 2021

Published 2021. This article is a U.S. Government work and is in the public domain in the USA.

Continental-Scale Geographic Trends in Barometric-Pumping Efficiency Potential: A North American Case Study

Sofia T. Avendaño¹ , Dylan R. Harp¹ , Sudarshan Kurwadkar^{2,3} , John P. Ortiz^{1,4} , and Philip H. Stauffer¹ 

¹Los Alamos National Laboratory, Los Alamos, NM, USA, ²California State University, Fullerton, CA, USA, ³U. S. Environmental Protection Agency, Ada, OK, USA, ⁴The Johns Hopkins University, Baltimore, MD, USA

Abstract Barometric pumping is a gas transport mechanism that has important implications for many applications involving subsurface gas seepage processes. This study provides the first continental-scale analysis of barometric-pumping efficiency potential based on meteorology. We quantified the barometric-pumping efficiency potential at 1,257 locations across the continental US and Canada. The results provide continental-scale geographic dependencies of barometric-pumping efficiency potential, indicating a significant correlation with latitude and a nonlinear dependence on longitude. The analysis also indicates that variability in barometric-pumping efficiency potential decreases with distance from the coast and as elevation increases. Locations far from the coastline are more likely to have upper mid-range potentials, while higher elevation locations are more likely to have low potentials. The highest barometric-pumping efficiency potentials are mostly found around the Gulf of St. Lawrence around 50°N. Locations along the Atlantic coast exhibit large-scale variations in potentials with a clear increasing trend with latitude.

Plain Language Summary We calculate the potential for variations in barometric pressure at different geographic locations to extract air and other gases from underground to the ground surface. This process is known as barometric pumping, an important process in various applications including underground gas leakage, radon gas entry into structures, and contaminated soil remediation. In this study, we evaluate the influence of latitude, longitude, elevation, and distance from the coast on the potential for barometric pumping based solely on atmospheric pressure records across North America (referred to as “potential” here for brevity). We find that latitude has the greatest effect on potential and that the highest potentials are found around the Gulf of St. Lawrence around 50°N. We also find that variability in potential decreases further from the coast and with high elevations. Generally, more eastern longitudes have higher potentials than central and western longitudes for the same latitudes.

1. Introduction

Barometric pumping is a natural process that drives gas transport from underground to the ground surface as the atmospheric pressure fluctuates. When barometric pressure increases, it pushes atmospheric air into the subsurface. Then as barometric pressure decreases, it pulls the subsurface gases up toward the surface. In effect, along with other processes such as thermal convection (Nachshon et al., 2008; Weisbrod et al., 2009), wind (Colbeck, 1989; Laemmel et al., 2017; Nachshon et al., 2012), and topographic effects (Weeks, 2001), barometric pumping is one of the drivers of subsurface “breathing” causing air exchange between the atmosphere and subsurface (Nilson et al., 1991). This process is most effective in porous media with preferential flow paths such as open fractures (Stauffer et al., 2019). Barometric-pumping efficiency is a measure of the ability of barometric pressure components (individual sinusoids composing the barometric record) to drive air exchange between the atmosphere and subsurface. It takes into account the component’s frequency, ability to drive air into the subsurface, and ability to extract contaminated air from the subsurface to the atmosphere (Harp et al., 2019). Since geologic properties and fracture characteristics vary at significantly smaller spatial scales than atmospheric pressures, we limit this analysis to the atmospheric potential of barometric-pumping efficiency at each site, referred to as “potential” for brevity hereafter.

Many subsurface applications are concerned with gas transport driven by barometric pumping. Some examples include passive soil vapor extraction (Neeper & Stauffer, 2012; You et al., 2010), nuclear test ban treaty verification (Bourret et al., 2020; Carrigan et al., 1996; Jordan et al., 2014; Olsen et al., 2016), estimating aquifer properties (Fuentes-Arreazola, et al., 2018), and estimating air permeability in soils (Lu, 1999; Weeks, 1978). Barometric pumping also plays a role in greenhouse gas emission leakage from abandoned wells (Levintal et al., 2018, 2020), CO₂ leakage from snowpack and soils (Massman, 2006), methane from landfills (Christophersen et al., 2001), and to a small extent water vapor from fractured rock (Martinez & Nilson, 1999). It also affects leakage of radon from alluvium (Clements & Wilkening, 1974) and natural gas from oil and gas boreholes (Forde et al., 2019). Kuang et al. (2013) provide a review of different applications affected by barometric pumping. While there have been many studies investigating the physical process of barometric pumping concerning these applications, there has not, to our knowledge, been a large-scale analysis of geographic trends in potential. Our analysis can inform industrial and environmental processes concerned with subsurface gas transport potential at different locations. Geologic conditions (e.g., average fracture aperture, matrix porosity, and matrix permeability) can be easily integrated into the analysis to further refine the estimate of efficiency for specific geologic settings near the locations in our analysis (Harp et al., 2019).

Harp et al. (2019) developed an analytical approach based on analytical solutions derived by Nilson et al. (1991) that quantifies barometric-pumping efficiency for fractured media. Using barometric records from Anchorage, Alaska (AK), Harp et al. (2019) demonstrated that the analytical approach produced results that are consistent with an independent inverse numerical analysis that identified a characteristic component, a single sinusoid over time defined by a period and amplitude that produces nearly identical gas transport as the actual barometric record. Harp et al. (2020) used a similar analytical approach to discriminate between historic events that led to gas seepage versus those that did not at what is now the National Nuclear Security Site in southern Nevada, United States (US), a study that focused on geologic conditions within a localized geographic area (16 locations within an $\sim 15 \times 15$ km² area). The study indicated that geologic differences even within a localized geographic area can cause significant differences in individual component barometric-pumping efficiencies.

In this study, we apply a similar methodology to a large set of US and Canadian locations to determine how barometric differences across geographic locations affect potential. We look at the relative differences between statistical metrics of the distribution of potentials at the locations and their associated representative periods and amplitudes. While we ensure that the representative period for Anchorage, AK is consistent with Harp et al. (2019), we do not verify that the periods and amplitudes are *characteristic* periods and amplitudes for all locations in our study. Instead, we focus on the relative differences between locations to identify geographic dependencies and refer to the potentials, periods, and amplitudes as *representative*. It has long been recognized that barometric signals generally have greater amplitudes at higher latitudes, suggesting that potentials will increase with latitude; however, we find that the highest potentials occur around 50°N in North America. We also investigate the dependence of potential on longitude, distance from the coast, and elevation.

2. Methods

For each geographic location in our analysis, we first decomposed the barometric-pressure record into a distribution of individual sinusoidal components defined by their period (period = $2\pi/\text{frequency}$) and amplitude using a Fast Fourier Transform. Then we quantified the atmospheric potential for barometric-pumping efficiency of each barometric component using the approach from Harp et al. (2019) by finding the diffusive efficiency and breathing efficiency associated with each component.

Barometric pumping depends on geologic properties such as fracture and rock properties (Harp et al., 2020; Nilson et al., 1991), which can vary greatly across regional and even local scales; however, we use constant geologic properties across all locations to focus on large-scale geographic trends based on meteorological differences. We used a geologically homogenous subsurface with a porosity of 30% and rock matrix permeability of $1\text{e}-16$ m², which is within the typical range of sandstone, limestone, and tuff (Freeze & Cherry, 1979; INTERA, 1983). We used a depth to the water table of 100 m which is very deep for water table

depths in North America (greater than 80 m; Fan et al., 2013; Miguez-Macho et al., 2008), but this depth occurs at least in the western United States (Lopes et al., 2006; SGMA GW, 2020; Snyder, 2008) and is within the range affected by barometric pumping (Neeper, 2002). Future analyses can refine our results by including water table depths, although considering that water table depths can vary significantly even at one location, this will require a much larger effort than our study. We use a fracture spacing of 10 m, which is considered an extremely wide fracture spacing (USBR, 2001) allowing ample rock matrix storage effects to be included in the analysis. We used a value of 1 mm fracture aperture, which is within the range of moderately open fracture apertures (1–3 mm; USBR, 2001).

Meteorological differences can vary on the microscale to synoptic scale (e.g., between 2,000 and 10,000 km for baroclinic waves, and between 200 m and 2 km for tornadoes; Orlandi, 1975) while Shokri et al. (2019), reviewed a variety of studies with horizontal spatial correlation lengths between 0.92 and 3,700 m so the meteorologic spatial scale can often be greater than the geologic spatial scale. To be able to estimate gas flux at a given location, one would need to account for the geologic properties of the site as well. However, in our case, other choices for geologic properties are not expected to significantly alter the relative comparisons of the potential provided by our analysis.

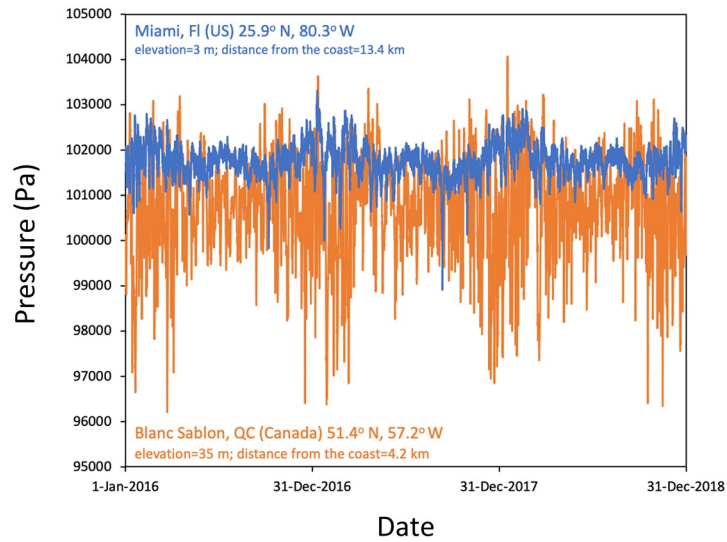
Next, we identified the representative components associated with high potentials for each location (i.e., the components responsible for the vast majority of the gas transport). We calibrated to the known characteristic period of Anchorage from the independent numerical inverse analysis in Harp et al. (2019), of 7.3 days. We first sorted the amplitudes and periods by decreasing potential and calculated the rolling mean of the sorted periods, amplitudes, and potentials with a window size of 60 to smooth the data. Smoothing the data with a window size of 60 was the smallest window that still allowed us to match the known characteristic period of Anchorage. Smaller windows could not result in a characteristic period of 7.3 days likely because high-potential, subdiurnal periods tended to overshadow the average. Keeping the window as small as possible allowed us to avoid over-smoothing the data. We then took the average of the period and amplitude distributions weighted by transformed potentials to emphasize the high-potential components. To ensure that the results are consistent with Harp et al. (2019), which were confirmed by a numerical inverse analysis, we nonlinearly transformed the potentials ($\mathbf{y} = \mathbf{x}^{12.5}$, where \mathbf{x} are the calculated potentials and \mathbf{y} are the transformed potentials used as weights) to scale the efficiencies to match the characteristic period of 7.3 days for Anchorage, Alaska. To calculate the representative potential at each location, we took the average of the 130 highest smoothed potentials (top 1%) to focus on the components responsible for most of the gas transport at each location (Harp et al., 2020). See supporting information for more discussion.

3. Data

We compiled 3-years barometric pressure records (altimeter setting data) from January 1, 2016, to December 31, 2018, for all locations from the Iowa State University ASOS airport weather data network (<https://mesonet.agron.iastate.edu/>). We converted from altimeter setting to station pressure using MetPy (May et al., 2020). We filtered the locations by the following criteria: (a) availability of three years of data, (b) $\leq 1\%$ of the data were missing, (c) the values were within a reasonable range of less than 108.4 kPa and more than 86.4 kPa (values lower than 91.4 kPa or higher than 106.7 kPa were manually checked and deleted if they were outliers because these would be unreasonably high or low values) and (d) no more than 7 consecutive days of data were missing. We obtained a uniform temporal data spacing of 1 h using linear interpolation; locations with data that could not be interpolated for the full 3 years (different start or end times) were not included. We obtained distances to coastlines from NASA's Ocean Biology Processing Group (<https://oceancolor.gsfc.nasa.gov/docs/distfromcoast/>) with distances provided as discrete points on a 0.04° grid. The point closest to each location was chosen.

As is apparent in our analysis, the locations are not evenly distributed spatially since cities may have multiple available records, while rural and especially mountainous areas will likely have fewer. As a result, there is an increased density of locations in the eastern US and sporadic coverage in the Rocky Mountain region, Canada and Alaska. Using station pressure converted from altimeter setting relies on accurate data for elevations (Sorenson & Pauley, 2019). We used the elevations provided by the Iowa State website which generally relies on a DEM with a resolution of 92.5 m (in the ESRI Elevation World MapServer) because station

a) Barometric Pressure Records for Min and Max Potential Locations



b) Histograms of Potentials for Min and Max Locations

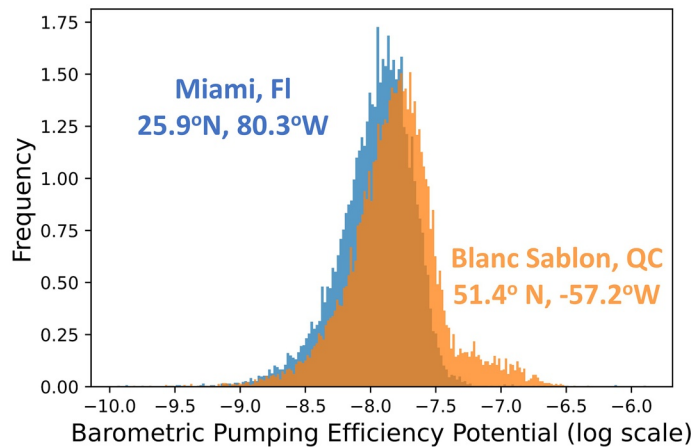


Figure 1. (a) Barometric station pressure records (elevation taken into account) and (b) histograms of barometric-component potentials for locations with the highest (Blanc Sablon, QC, Canada) and lowest (Miami, FL, US) representative potential.

output does not give the elevation. ASOS stations are usually located in or near airports, so our data is generally from flatter areas. Elevation errors affect high elevation locations more than lower-elevation locations. Also, restricting our analysis to the continental US and Canada means that we only considered locations in the northern hemisphere with latitudes between 24.6° and 80.0°N. Mexico was not included because only two locations had data that matched our criteria above. Therefore, while we expect that the general trends in our results may apply to other continents, the details of the analysis are likely specific to North America.

4. Results

Figure 1 depicts the barometric records and associated barometric-component potential distributions for the locations with the highest and lowest representative potentials to illustrate the end-member locations in the data set. The distributions contain the potentials for all components extracted from the barometric records. The lowest representative potential location is Miami, FL, US (25.9°N, 80.3°W), while the highest is Blanc Sablon, QC, Canada (51.4°N, 57.2°W). The locations are on the Atlantic Coast, with Blanc Sablon located on the Gulf of St. Lawrence in eastern Quebec while Miami is on the southeastern end of Florida.

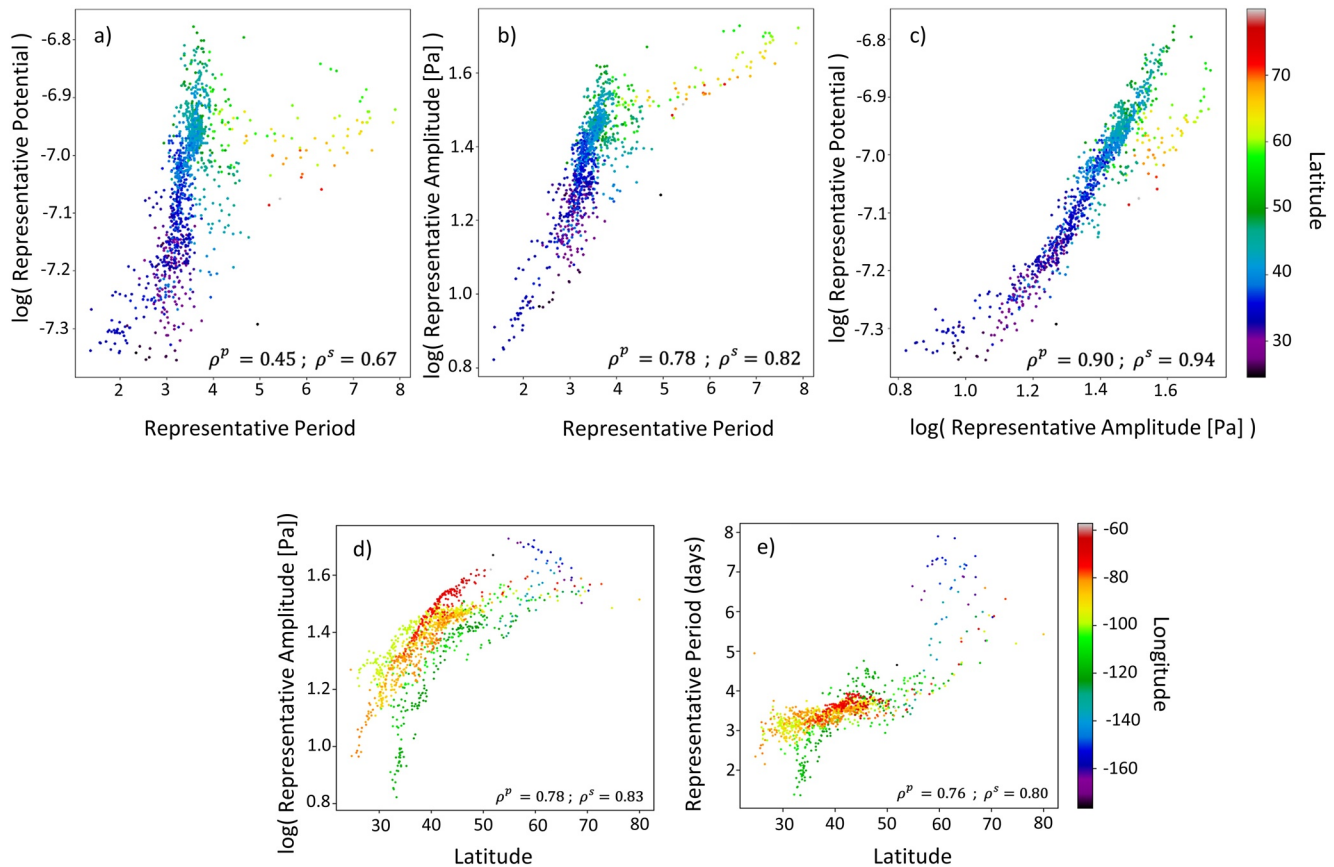


Figure 2. Comparisons of (a) barometric-pumping efficiency potential with the representative period, (b) representative amplitude with the representative period, and (c) representative barometric-pumping efficiency potential with representative amplitude. Colorbar indicates latitude. (d) Representative amplitude and (e) representative period with latitude. Colorbar indicates longitude.

The barometric records as shown in Figure 1a indicates that Blanc Sablon has a much larger barometric amplitude, whereas Miami is generally much more quiescent. In Figure 1b, the distribution of barometric-component potentials for Blanc Sablon is shifted toward higher values and has a thicker right tail compared to Miami.

Figure 2 contains scatterplots between the representative potentials, representative periods, and representative amplitudes (referred to simply as potentials, periods, and amplitudes for the remainder of this section). The highest potentials are associated with a period between 3 and 4 days located around 50°N in North America (Figure 2a). Amplitude versus period (Figure 2b) shows a change in slope around 4 days (50°N) but, in general, does continue to increase with the period after that. Most of the periods are between 3 and 4 days, with an almost vertical slope for potentials (Figure 2a) and, to a lesser extent, amplitudes (Figure 2b) for these locations. Locations with latitudes > 60°N typically have periods between 5 and 8 days. The Pearson (ρ^p) and Spearman (ρ^s) coefficients of 0.78/0.82 between amplitude and period indicate a strong linear correlation which is obvious in Figure 2b. Potential is highly correlated with amplitude ($\rho^p = 0.90$, $\rho^s = 0.94$; Figure 2c) and to a lesser extent with a period ($\rho^p = 0.45$, $\rho^s = 0.67$; Figure 2a).

The bottom row of plots in Figure 2 contains scatterplots between amplitude and potential (Figure 2d) and period and potential (Figure 2e). Latitude has high Pearson and Spearman correlation coefficients with both periods ($\rho^p = 0.78$, $\rho^s = 0.83$) and amplitude ($\rho^p = 0.76$, $\rho^s = 0.80$). Although the Pearson coefficients are high for both, the plots suggest some nonlinearity in the correlation. Period versus longitude also has a somewhat significant Pearson coefficient at -0.38 , although the Spearman correlation is negligible with a coefficient of -0.02 .

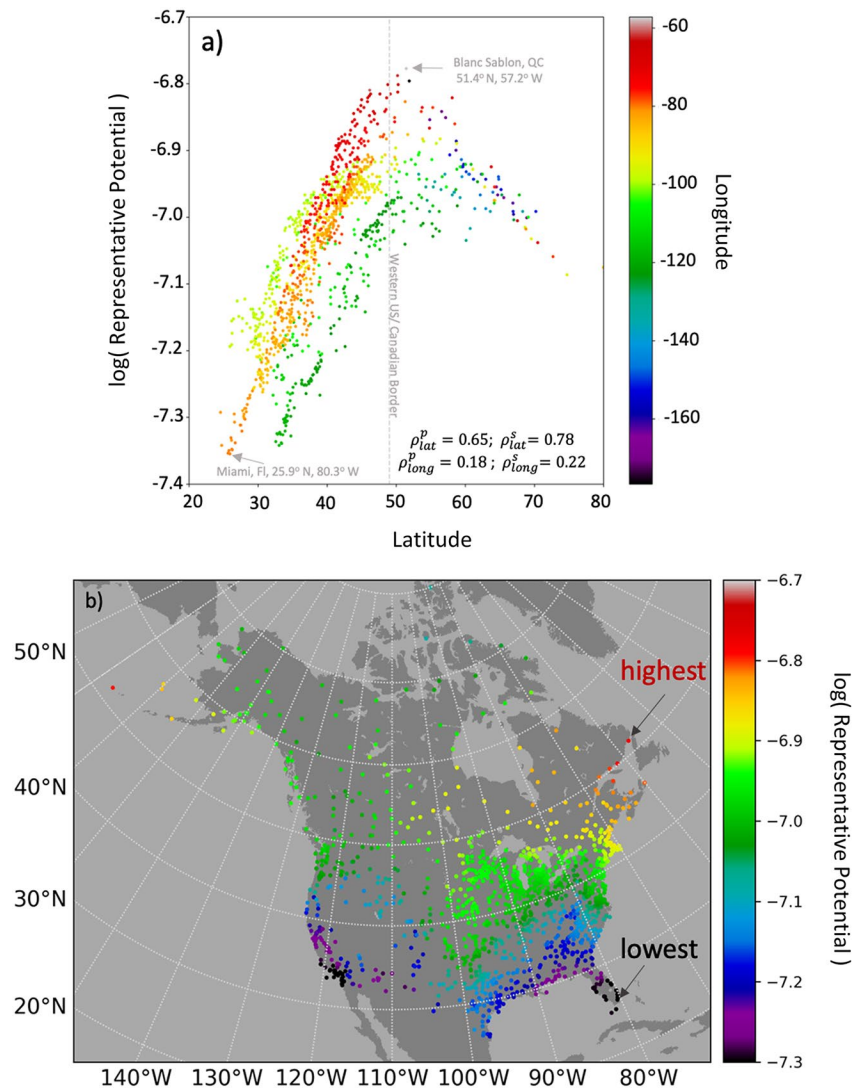


Figure 3. (a) Potential as a function of latitude. Colors indicate longitude. (b) Map of barometric-pumping efficiency potentials. The locations with the highest and lowest potentials are indicated.

For latitude versus potential, a Pearson's correlation coefficient of 0.65 suggests that the latitude is linearly correlated with potential, while a Spearman's coefficient of 0.78 suggests a stronger monotonic correlation (Figure 3a). Despite positive linear and a monotonic correlation between latitude and potential, a scatterplot between the two indicates that the dependence is better described by a concave nonlinear relationship with a maximum of around 50°N (Figure 3a). The bias in the data toward lower latitudes is also apparent in Figure 3a. A linear fit between latitude and potential gives an R-squared value of 0.43, while a parabolic fit gives an R-squared value of 0.63. While longitude does not exhibit a strong linear or monotonic correlation with potential ($\rho^p = 0.18$, $\rho^s = 0.22$), the structure is apparent in overlapping clusters of locations with similar longitude in Figure 3a, indicating a more complicated dependence exists than linear and monotonic correlation metrics can identify. For example, there are clusters of locations with longitudes around 70–80°W (red points), 80–90°W (orange points), and 115–125°W (green points). Generally, the west coast has lower potentials than the east coast for equivalent latitudes. Central locations have the highest potentials at latitudes less than 40°N. The highest potentials overall are located around the Gulf of St. Lawrence (~40–50°N and 55–70°W; Figure 3b). Interestingly, Blanc Sablon is the easternmost site and has the highest potential. Extreme western longitudes in Alaska around 50°N also have high potentials. For locations north of 50°N,

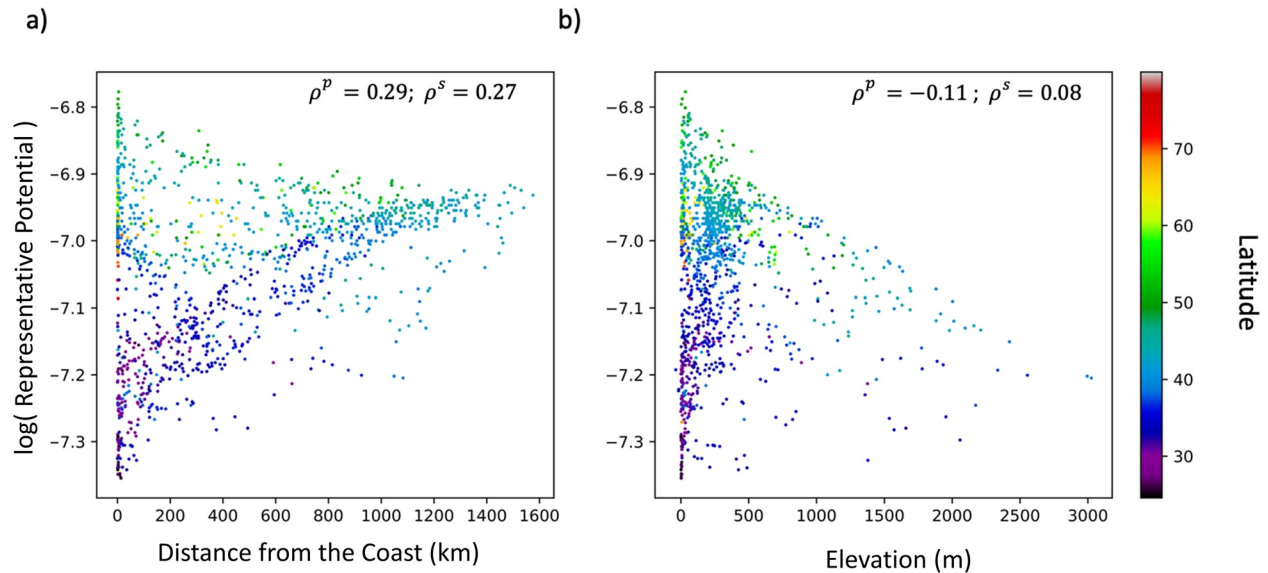


Figure 4. Potential as a function of (a) distance from the coast and (b) elevation. Colorbar indicates latitude in both plots.

where the potentials begin to decline, the trends associated with longitude for locations less than 50°N become less clear; however, there are also significantly fewer data in this area.

Despite low linear and monotonic correlations for distance to coastline and elevation, scatterplots between these factors and potential exhibit striking structural dependencies. Note that elevation and distance to the coastline are strongly monotonically correlated with Spearman's correlation coefficient of 0.73 (Pearson's coefficient of 0.46) because geographical locations with low elevations are often found near coastlines, while the higher elevations often tend to be farther inland. This may also be partly caused by the fact that we used airport locations, which are most likely to be situated in flatter areas (valleys) rather than in mountainous areas. So locations such as mountains near the coast are not likely to be included in our analysis. In North America, locations farthest from the coastline are between 40 and 50°N, which is also a latitude band associated with high potential. Coastal locations have a wide range of potentials (Figure 4a). An apparent trend is that as the distance from coastlines increases, potentials become generally constrained within a narrowing band. This indicates that inland locations have less variability in potential than coastal locations where potentials clearly increase with latitude (e.g., the Atlantic Coast in Figure 4b). Elevation has very low correlation coefficients, indicating that it is not linearly or monotonically correlated with potential; however, there is a steep decrease in the upper bound of potential as elevation increases. In other words, higher elevations have lower maximum possible potential and a narrower range in potentials.

5. Discussion

We identified the geographic factors driving potential on a continental scale using locations across the US and Canada. Besides an enhanced understanding of passive atmospheric/subsurface air exchange, understanding the influence of these factors on a continental scale has many applications. This study can be used to assess geographic differences in barometric-pumping efficiency potential for passive, contaminated-soil remediation efforts and the risk of unwanted barometrically induced gas transport such as CO₂ leakage from geologic storage sites, radon gas entry into structures, and methane leakage during natural gas extraction operations. The representative period can be calculated at a given location using readily available barometric records to find a quick estimate of the dominant time interval of barometric pumping and gas transport at a location aiding gas seepage site monitoring plans and in predictive transport modeling. This study is based solely on differences in barometric records between geographic locations and does not consider geologic conditions. While geologic conditions, such as rock-matrix permeability, will not affect iden-

tifying the representative component (Harp et al., 2019), they will undoubtedly affect individual component potentials and will vary at smaller spatial scales than meteorological conditions.

We developed a nonlinear-weighting scheme based on barometric component potential to ensure that our findings are consistent with the characteristic period of 7.3 days for Anchorage, AK (61°N) from Harp et al. (2019), which was identified using an independent inverse numerical approach. While previous research has speculated that barometric pumping is predominantly driven by weekly time-frame barometric components caused by weather patterns (~7 days; Nilson et al., 1991; Neeper, 2003; Mourzenko et al., 2014), our results indicate that while this is likely true at high-latitudes, dominant periods may be significantly shorter at lower latitudes. Most representative periods for latitudes less than 50°N were between 3-4 days. Both the representative amplitude and period (Figure 2b) generally increase as latitude increases. This indicates a strong correlation between representative amplitude and period consistent with the findings in Harp et al. (2020). Interestingly, there is a considerable decrease in potential for higher latitudes (Figure 2a), indicating a reversal in trend around 50°N, a feature that is, also reflected in a distinct change in slope for amplitudes versus periods (Figure 2b).

There is a clear increasing trend in potentials along the Atlantic coast (Figure 3b) and to a lesser extent along the Pacific coast as you increase latitude until around 50°N. For the Atlantic coast, this trend is mostly linear from Florida to the Gulf of St. Lawrence. Low latitude locations along the Pacific coast have low potentials until around 43°N, where potentials are intermediate up to 60°N and increases along the Alaskan coast. The Arctic coast has stable potentials, possibly because it is predominantly aligned east-west so that latitude is nearly constant. Winter pressure variability caused by winter storm tracks is also greatest along the midlatitude coasts, especially along the Atlantic Coast, which may explain why we see high potentials along the Gulf of St. Lawrence and lower Alaskan islands (Michaelis et al., 2019). Inland locations farther from the coast have much less variability (i.e., smaller ranges of potentials), while central locations have their highest potentials for latitudes less than 40°N (i.e., the southern portion of the US). This has important implications for the potential for barometric pumping, where particularly along the Atlantic coastline, the potential will largely depend on latitude, while latitude will be less critical for inland locations. Another important finding is that maximum potential decreases as locations increase in elevation. In other words, while low elevations have a wide range of potentials, higher elevations become increasingly restricted to lower potentials.

6. Conclusions

- Latitude is the dominant factor controlling geographic trends in potential. This dependence is striking along the Atlantic coast and apparent to a lesser degree along the Pacific coast. The range in potentials for a given latitude decreases at locations farther from coastlines, indicating less variability in potential within continental interiors
- Potential appears to have a concave nonlinear dependence on latitude in North America. Potential increases with North American latitudes until around 50°N, after which it begins to decrease
- Representative period and amplitude (associated with high-efficiency barometric components) increase as latitude increases. This is consistent with the fact that, in general, barometric signals are noisier at higher latitudes
- Longitude is a less dominant factor than latitude in potential. For latitudes, less than 40°N, mid-longitude North American locations generally have their highest potentials, followed by eastern and western locations. Generally, the east coast exhibits higher potentials for a given latitude than the west coast
- While low elevation locations have a wide range in potentials, as elevation increases, the maximum potentials, and their range decrease

Data Availability Statement

The barometric record data and data retrieval script was from the Iowa State University ASOS website (<https://mesonet.agron.iastate.edu/>). The coastal distance data was from NASA's Ocean Biology Processing Group (<https://oceancolor.gsfc.nasa.gov/docs/distfromcoast/>).

Acknowledgments

This research is supported by the National Nuclear Security Administration Office of Defense Nuclear Nonproliferation Research and Development (NNSA DNN R&D). Los Alamos National Laboratory completed this work under the auspices of the U.S. Department of Energy under contract DE-AC52-06NA24596 and 89233218CNA000001. The authors acknowledge important interdisciplinary collaboration with scientists and engineers from LANL, LLNL, MSTs, PNNL, and SNL. Sudarshan Kurwadkar was supported through the Visiting Faculty Program sponsored and managed by the DOE Office of Science's Office of Workforce Development for Teachers and Scientists (WDTS) collaboration with the DOE laboratories.

References

- Bourret, M. S., Kwicklis, E. M., Harp, D. R., Ortiz, J. P., & Stauffer, P. H. (2020). Beyond Barnwell: Applying lessons learned from the Barnwell site to other historic underground nuclear tests at Pahute Mesa to understand radioactive gas-seepage observations. *Journal of Environmental Radioactivity*, 222, 106297. <https://doi.org/10.1016/j.jenvrad.2020.106297>
- Carrigan, C. R., Heinle, R. A., Hudson, G. B., Nitao, J. J., & Zucca, J. J. (1996). Trace gas emissions on geological faults as indicators of underground nuclear testing. *Nature*, 382, 528–531. <https://doi.org/10.1038/382528a0>
- Christophersen, M., Kjeldsen, P., Holst, H., & Chanton, J. (2001). Lateral gas transport in soil adjacent to an old landfill: Factors governing emissions and methane oxidation. *Waste Management & Research*, 19, 595–612. <https://doi.org/10.1177/0734242X0101900616>
- Clements, W. W., & Wilkening, M. H. (1974). Atmospheric pressure effects on 222Rn transport across the earth-air interface. *Journal of Geophysical Research*, 79(33), 5025–5029. <https://doi.org/10.1029/JC079i033p05025>
- Colbeck, S. C. (1989). Air ovement in snow due to windpumping. *Journal of Glaciology*, 35(120), 209–213. <https://doi.org/10.3189/S0022143000004524>
- Fan, Y., Li, H., & Míguez-Macho, G. (2013). Global patterns of groundwater table depth. *Science*, 339, 940–943. <https://doi.org/10.1126/science.1229881>
- Forde, O. N., Cahill, A. G., Beckie, R. D., & Mayer, K. U. (2019). Barometric-pumping controls fugitive gas emissions from a vadose zone natural gas release. *Scientific Reports*, 9, 14080. <https://doi.org/10.1038/s41598-019-50426-3>
- Freeze, R. A., & Cherry, J. A. (1979). *Groundwater*. University of Michigan.
- Fuentes-Arreazola, M. A., Ramírez-Hernández, J., & Vázquez-González, R. (2018). Hydrogeological properties estimation from groundwater level natural fluctuations analysis as a low-cost tool for the Mexicali Vally Aquifer. *Water*, 10(5), 586. <https://doi.org/10.3390/w10050586>
- Harp, D. R., Bourret, M. S., Stauffer, P. H., & Kwicklis, E. M. (2020). Discriminating underground nuclear explosions leading to late-time radionuclide gas seeps. *Geophysical Research Letters*, 47, e2019GL086654. <https://doi.org/10.1029/2019GL086654>
- Harp, D. R., Ortiz, J. P., & Stauffer, P. H. (2019). Identification of dominant gas transport frequencies during barometric pumping of fractured rock. *Scientific Reports*, 9(1), 9537. <https://doi.org/10.1038/s41598-019-46023-z>
- INTERA. (1983). *Porosity, permeability, and their relationship in Granite, Basalt, and tuff*, Technical Report, April 1983. INTERA Environmental Consultants, Inc. Retrieved from <https://www.osti.gov/servlets/purl/6116963>
- Jordan, A. B., Stauffer, P. H., Zyvoloski, G. A., Person, M. A., MacCarthy, J. K., & Anderson, D. N. (2014). Uncertainty in prediction of radionuclide gas migration from underground nuclear explosions. *Vadose Zone Journal*, 13, 1–13. <https://doi.org/10.2136/vzj2014.06.0070>
- Kuang, X., Jiao, J. J., & Li, H. (2013). Review on airflow in unsaturated zones induced by natural forcings. *Water Resources Research*, 49, 6137–6165. <https://doi.org/10.1002/wrcr.20416>
- Laemmel, T., Mohr, M., Schack-Kirchner, H., Schindler, D., & Maier, M. (2017). Direct observation of wind-induced pressure-pumping on gas transport in soil. *Soil Science Society of America Journal*, 81(4), 770–774. <https://doi.org/10.2136/sssaj2017.01.0034n>
- Levintal, E., Dragila, M. I., Zafir, H., & Weisbrod, N. (2020). The role of atmospheric conditions in CO₂ and radon emissions from an abandoned water well. *The Science of the Total Environment*, 722, 137857. <https://doi.org/10.1016/j.scitotenv.2020.137857>
- Levintal, E., Lensky, N. G., Mushkin, A., & Weisbrod, N. (2018). Pipes to Earth's subsurface: The role of atmospheric conditions in controlling air transport through boreholes and shafts. *Earth System Dynamics*, 9(3), 1141–1153. <https://doi.org/10.5194/esd-9-1141-2018>
- Lopes, T. J., Buto, S. G., LaRue Smith, J., & Welborn, T. L. (2006). *Water table depths and gradients, Nevada, 1947–2004*. (pp. 2006–5100). USGS and Department of Interior Scientific Investigations Report. Retrieved from https://pubs.usgs.gov/sir/2006/5100/pdf/SIR2006_5100.pdf
- Lu, N. (1999). Time-series analysis for determining vertical air permeability in unsaturated zones. *Journal of Geotechnical and Geoenvironmental Engineering*, 125(1), 69–71. [https://doi.org/10.1061/\(asce\)1090-0241\(1999\)125:1\(69\)](https://doi.org/10.1061/(asce)1090-0241(1999)125:1(69))
- Martinez, M. J., & Nilson, R. H. (1999). Estimates of barometric pumping of moisture through unsaturated fractured rock. *Transport in Porous Media*, 36, 85–119. <https://doi.org/10.1023/A:1006593628835>
- Massman, W. J. (2006). Advective transport of CO₂ in permeable media induced by atmospheric pressure fluctuations: 1. An analytical model. *Journal of Geophysical Research*, 111, G03004. <https://doi.org/10.1029/2006JG000163>
- May, R. M., Arms, S. C., Marsh, P., Bruning, E., Leeman, J. R., Goebbert, K., et al., 2020: *MetPy: A python package for meteorological data. Unidata*. <https://doi.org/10.5065/D6WW7G29>
- Michaelis, A. C., Lackmann, G. M., & Robinson, W. A. (2019). Evaluation of a unique approach to high-resolution climate modeling using the model for prediction across scales – atmosphere (MPAS-A) version 5.1. *Geoscientific Model Development*, 12, 3725–3743. <https://doi.org/10.5194/gmd-12-3725-2019>
- Míguez-Macho, G., Li, H., & Fan, Y. (2008). Simulated water table and soil moisture climatology over North America. *Bulletin of the American Meteorological Society*, 89, 663–672. <https://doi.org/10.1175/bams-89-5-663>
- Mourzenko, V., Varloteaux, C., Guillon, S., Thovert, J. F., Pili, E., & Adler, P. M. (2014). Barometric pumping of a fractured porous medium. *Geophysical Research Letters*, 41, 6698–6704. <https://doi.org/10.1002/2014GL060865>
- Nachshon, U., Dragila, M., & Weisbrod, N. (2012). From atmospheric winds to fracture ventilation: Cause and effect. *Journal of Geophysical Research*, 117(G2), G02016. <https://doi.org/10.1029/2011JG001898>
- Nachshon, U., Weisbrod, N., & Dragila, M. I. (2008). Quantifying air convection through surface-exposed fractures: A laboratory study. *Vadose Zone Journal*, 7, 948–956. <https://doi.org/10.2136/vzj2007.0165>
- Neeper, D. A. (2002). Investigation of the vadose zone using barometric pressure cycles. *Journal of Contaminant Hydrology*, 54, 59–80. [https://doi.org/10.1016/s0169-7722\(01\)00146-2](https://doi.org/10.1016/s0169-7722(01)00146-2)
- Neeper, D. A. (2003). Harmonic analysis of flow in open boreholes due to barometric pressure cycles. *Journal of Contaminant Hydrology*, 60, 135–162. [https://doi.org/10.1016/s0169-7722\(02\)00086-4](https://doi.org/10.1016/s0169-7722(02)00086-4)
- Neeper, D. A., & Stauffer, P. H. (2012). Transport by oscillatory flow in soils with rate-limited mass transfer II. *Field Experiment Vadose Zone Journal* 11(2), vzj2011.0094. <https://doi.org/10.2136/vzj2011.0094>
- Nilson, R. H., Peterson, E. W., Lie, K. H., Burkhard, N. R., & Hearst, J. R. (1991). Atmospheric pumping: A mechanism causing vertical transport of contaminated gases through fractured permeable media. *Journal of Geophysical Research*, 96(B13), 21933–21948. <https://doi.org/10.1029/91jb01836>
- Olsen, K. B., Kirkham, R. R., Woods, V. T., Haas, D. H., Hayes, J. C., Bowyer, T. W., et al. (2016). Noble gas migration experiment to support the detection of underground nuclear explosions. *Journal of Radioanalytical and Nuclear Chemistry*, 307, 2603–2610. <https://doi.org/10.1007/s10967-015-4639-7>
- Orlanski, I. (1975). A rational subdivision of scales for atmospheric processes. *Bulletin of the American Meteorological Society*, 56(5), 527–534. <https://doi.org/10.1175/1520-0477-56.5.527>

- SGMA. (2020). *USGS periodic GW measurements, Spring 2020*. Department of Water Resources SGMA Portal. Retrieved from <https://sgma.water.ca.gov/webgis/?appid=SGMADataViewer#gwlevels>
- Shokri, S., Shademan, M., Rezvani, M., Javankhoshdel, S., Cami, B., & Yacoub, T. (2019). *A review study about spatial correlation measurement in rock mass. Paper presented at 14th International Congress on Rock Mechanics and Rock Engineering (ISRM 2019)*. Foz do Iguassu, Brazil.
- Snyder, D. T. (2008). *Estimated depth to ground water and configuration of the water table in the Portland, Oregon area* (pp. 2008–5059). USGS Scientific Investigations Report. Retrieved from <http://pubs.usgs.gov/sir/2008/5059>
- Sorenson, B., & Pauley, P. M. (2019). *Effects of elevation errors on the calculation of station pressure. Poster presented at the 99th annual meeting of the American meteorological Society*. Phoenix, AZ.
- Stauffer, P. H., Rahn, T., Ortiz, J. P., Salazar, L. J., Boukalfa, H., Behar, H. R., & Snyder, E. E. (2019). Evidence for high rates of gas transport in the deep subsurface. *Geophysical Research Letters*, *46*(7), 3773–3780. <https://doi.org/10.1029/2019GL082394>
- USBR (2001). *U. S. Bureau of Reclamation, Engineering Geology Field Manual* (2nd ed., Vol. 1, 1998). Retrieved from <https://www.usbr.gov/tsc/techreferences/mands/geologyfieldmanual-vol1/GeolMan-v1-all.pdf>
- Weeks, E. P. (1978). *Field determination of vertical permeability to air in the unsaturated zone*. U.S. Geol. Surv. Prof. Pap., 1051. <https://doi.org/10.3133/pp1051>
- Weeks, E. P. (2001). Effects of Topography on Gas Flow in Unsaturated Fractured Rock: Concepts and Observations. *Flow and Transport through Unsaturated Fractured Rock* (Vol. 42, pp. 53–59). Geophysical Monograph Series. <https://doi.org/10.1029/GM042p0053>
- Weisbrod, N., Dragila, M. I., Nachshon, U., & Pillersdorf, M. (2009). Falling through the cracks: The role of fractures in Earth-atmosphere gas exchange. *Geophysical Research Letters*, *36*, L02401. <https://doi.org/10.1029/2008GL036096>
- You, K., Zhan, H., & Li, J. (2010). A new solution and data analysis for gas flow to a barometric pumping well. *Advances in Water Resources*, *33*, 1444–1455. <https://doi.org/10.1016/j.advwatres.2010.07.008>